Surface & Coatings Technology 394 (2020) 125865

Contents lists available at ScienceDirect

Surface & Coatings Technology

journal homepage: www.elsevier.com/locate/surfcoat

Enhanced corrosion resistance of cold-sprayed and shot-peened aluminum coatings on LA43M magnesium alloy

Fei-Fei Lu[a], Kai Ma[a], Cheng-Xin Li[a,*], Muhammad Yasir[b], Xiao-Tao Luo[a], Chang-jiu Li[a]

[a] State Key Laboratory for Mechanical Behavior of Materials, School of Materials Science and Engineering, Xi'an Jiaotong University, Xi'an, Shaanxi 710049, China
[b] Department of Materials Science &Engineering, Institute of Space Technology, Islamabad 44000, Pakistan

ARTICLE INFO

Keywords:
Cold spray
Shot peening
Al coating
EIS
Polarization
LA43M alloy

ABSTRACT

A facile and environment-friendly strategy is proposed to prepare dense, thin and antioxidant aluminum coatings on LA43M magnesium alloy via cold spraying and subsequent shot peening technologies. High-energy martensitic stainless steel particles are used to tamp the cold-sprayed coatings, which resulted in complete plastic deformation of Al particles and elimination of pores. The samples with shot-peened Al coating showed excellent corrosion resistance in electrochemical tests. Moreover, long-term salt spray and immersion test revealed that the shot-peened Al coating can effectively protect LA43M alloy from corrosion. Shot-peened Al coating offered promising and long term applications time in the harsh environment.

1. Introduction

Magnesium-lithium (Mg—Li) alloys exhibit remarkable potential in automotive, aerospace, and electronic industries due to their high specific strength, high stiffness, excellent electromagnetic shielding ability, and outstanding damping performance [1–3]. In particular, the utilization of Mg—Li alloys in the aerospace industry have not only reduced the weight of the satellite but also increased the payload and reduced the launch cost [3]. Unfortunately, the inferior corrosion performance of Mg-based alloys severely restricts their widespread application. Therefore, more research needs to be done to improve the corrosion resistance of the Mg-based alloys. Surface treatment is the most commonly used method to improve the surface properties of a substrate. These treatments include chemical conversion, anodization, micro-arc oxidation (MAO), electroplating, organic and composite coatings [4–10]. The key purpose of these strategies is to form an effective surface film and isolate the substrate from the corrosive medium. However, Li is highly chemically and electrochemically active. The surface of Mg—Li alloy can get corroded instantly in the solution and form a loose oxide film on the alloy surface [11]. Therefore, the traditional protective film formed in solution is not suitable for highly active Mg—Li alloys. An alternative solvent-free coating method is required for protecting Mg—Li alloys.

Cold spraying is a novel coating technology, where micron-sized particles are accelerated by a relatively low-temperature gas jet to a high velocity. These accelerated particles generate plastic deformation and results in the deposition of the high-speed particle at desired substrate [5,12–14]. Generally, the temperature of the cold spray process is low, which can prevent the deposited particles from reacting with the atmosphere gas. So, the deposited coating will not undergo the defects such as oxidation, phase transformation and crack formation [15]. It is worth mentioning that the cold spraying process does not require any solution, which ultimately prevents the surface of the Mg—Li alloy from being corroded by the solution. The Al and Al-based alloy powders are abundantly used as raw materials in cold spraying. The density of Al is lower than other commercial metals such as Cu, Ni and Zn, so the Mg—Li alloy components gains a very slight weight increment after preparing Al coatings. In addition, a dense aluminum oxide film is naturally formed on the Al surface, which can further prevent corrosion from the corrosive medium [16,17]. However, due to the cumulative deposition characteristics of the cold sprayed particles, insufficient deformation of particles will cause pores inside the coating, especially forming a porous layer on the upper surface of the coating [13]. The corrosion medium can easily pass from the voids in the porous layer towards the substrate and results in corrosion. Hence, it is necessary to eliminate the voids of pure Al coating on Mg—Li alloys for improving the corrosion resistance of Mg—Li alloys.

The deposition characteristics of cold spraying process result in a porous microstructure at the top region and a denser central and internal region [18]. The initially cold sprayed particles experience large deformation due to their accelerated contact with the substrate and impact from the following particles. However, the later deposited

* Corresponding author.
E-mail address: licx@mail.xjtu.edu.cn (C.-X. Li).

https://doi.org/10.1016/j.surfcoat.2020.125865
Received 19 February 2020; Received in revised form 27 April 2020; Accepted 28 April 2020
Available online 05 May 2020

particles can cause defects in the coating, thereby reducing the protective properties of the coating. A common method to densify the cold spray coating is to mix two different particles for deposition and the tamping effect of the hard particles can be incorporated to densify the cold sprayed coating [19–23]. Wei et al. have blended large-sized stainless steel (SS) particles and commercially available Al6061 powder to deposit a dense Al6061 coating on AZ31B substrate. As a result, dense coating with a porosity of only 0.4% has been achieved with 60% SS content [24]. This method has a limitation to obtain dense coatings with thickness lesser than 300 μm. Moreover, the deposition efficiency is lower than the conventional cold spraying process due to the erosion of shot peened particles. Zhou et al. have explained that the deposition angle of incoming particles always deviates from 90° because of cambered crater, which results in inferior deposition efficiency [25]. Therefore, it is necessary to explore a suitable technology to obtain a dense coating while ensuring high deposition efficiency. Shot-peening treatment has been reported in most studies to improve fatigue behavior of metals. This can also influence residual stress and enhance corrosion resistance of bulk metallic materials [26–29]. The shot peening treatment produces a plastic deformation layer on AZ31 and AZ91 surface with nano-sized α-Mg grains [30], thereby improving the corrosion resistance of the alloys compared with as-received AZ31 and AZ91 alloys. The tamping effect of shot peening treatment is more significant on cold sprayed coatings than the bulk materials. Hence, shot peening technology is suitable for preparing a cold sprayed coating with highly density and corrosion resistance.

In this study, a facile method is used to deposit dense, thin and corrosion-resistant aluminum films on LA43M Mg—Li alloys to get the advantages of cold-spraying and tamping effect, such as high dynamic energy and residual compressive stress. The tamping process significantly improves the quality of cold-sprayed coating and effectively protects the non-erosion of LA43M magnesium substrate. Martensitic stainless steel powder with high hardness and magnetic property was used for peening treatment which was recycled and reused during tamping. The microstructure and densification mechanism of the coatings have been systematically investigated. The long-term stability and the electrochemical corrosion behavior of the samples with two coatings before and after shot peening process have been studied in neutral salt solution.

2. Experimental

2.1. Materials

The gas atomized 1050 pure Al powders (You Xing Lian Nonferrous Metals, Beijing, China) and the 1Cr18 SS powder (Wei Guang Shot-peening material Co., Ltd. Wuxi, China) were used as feedstock powders. The 1050 pure Al powder is used to prepare cold-sprayed Al coating deposits and 1Cr18 SS powder is used for subsequent shot peening to strengthen the aluminum coating. The morphology and size distribution of Al powder and SS powders are shown in Figs. 1 and 2, respectively. The LA43M Mg—Li alloy plate (240 × 20 × 5 mm) was used as a substrate for cold spraying. The composition of LA43M substrate, Al powder and bulk Al is shown in Table 1.

2.2. Preparation of cold sprayed coating

The aluminum coating was deposited by an in-house cold spraying system (CS2000, Xi'an Jiaotong University, China) equipped with a convergent-divergent Laval nozzle with a throat diameter of 2 mm, an outlet diameter of 6 mm and a divergent section length of 100 mm. Prior to cold spraying, the LA43M substrate was sandblasted with an alumina grit at a compressed air pressure of 0.6 MPa. Sandblasting was done to obtain rough surface and ensure good bond of the coating with the substrate. Substrate was ultrasonically cleaned by using acetone for 10 min. During the cold spraying process, nitrogen was used as the accelerating and carrier gas. The detailed spraying parameters are summarized in Table 2.

2.3. Post shot peening treatment for cold sprayed pure Al coating

A schematic illustration of the cold spraying process and shot peening treatment is presented in Fig. 3 to illustrate the influence of shot peening on the deformation behavior of Al particles. Initially, the conventional cold spraying process was used to deposit Al particles on LA43M substrate, followed by subsequent shot peening treatment to obtain a dense Al coating. The velocity and temperature of the particles at the exit point of the accelerating gun were calculated and presented in Fig. 3. Subsequent shot peening particles plays a critical role in the formation of cold-sprayed coatings [31]. The kinetic energy of larger shot peening particles is mainly absorbed by the Al particles and converted into plastic deformation [25]. The shot peening particles did not get deposited on the coating surface due to low temperature and pressure. Compared to the conventional cold spraying Al coatings, the shot-peened Al coating possesses highly flattened Al particles, which are strongly adhered to the substrate. The coating porosity has been significantly reduced due to the tamping effect of shot-peening particles.

Generally, the thickness of the dense coating increased as the number of shot peening increased and the impact depth of one shot-peening pass is about 100 μm [32]. The thickness of as-prepared pure Al coating was ~300 μm, a dense and uniform thin aluminum coating was obtained after three passes of shot peening. The shot-peening process was also carried out using the same cold spray system and the nitrogen was also used as the accelerating and carrier gas. The temperature and pressure of the gas was 200 °C and 1 MPa, respectively. The feed rate of the shot-peening particles (1Cr18 SS powder) was 35 g/min. The standoff distance between the nozzle and the surface of LA43M substrate was 20 mm and gun traverse speed was 80 mm/s.

2.4. Coating characterization

The microstructure (cross-sectional) and surface morphology of the pure Al coating were observed by using scanning electron microscopy (SEM, MIRA3 LMH, TESCAN, Czech) equipped with energy-dispersive spectroscopy (EDS). The porosity of the as-deposited coating was estimated from the polished cross-sectional SEM images by using image analysis software. For each sample, ten different SEM images, at a magnification of 1000 X in backscattered electron (BSE) mode, were used for porosity calculations. Micro-Vickers hardness was measured every 60 μm from the polished cross-section of the coating.

2.5. Electrochemical characterization

The electrochemical properties of LA43M alloy, as-deposited pure Al-coated LA43M, shot-peened pure Al-coated LA43M and pure Al (bulk material) were obtained using a CS310 electrochemical workstation (Corrtest Instruments Co., Ltd., Wuhan, China). The investigations were conducted in a three-electrode cell system, using a reference saturated calomel electrode (SCE), counter platinum electrode (CPE) and working electrode (WE). The surface of the sample was polished before the test to eliminate the effect of the surface roughness, and then it was embedded by epoxy resin with an exposed area of 1 cm^2. The electrochemical test was performed in 3.5 wt% NaCl solution at room temperature. During the measurement, the open circuit potential (OCP) attained a stable value with increasing time. The potentiodynamic polarization (PDP) test was carried out at a scan rate of 0.5 mV/s. The corrosion potential and corrosion current density were obtained from the polarization curves by using Tafel fitting. Electrochemical impedance spectroscopy (EIS) was also carried out at OCP, in the frequency range from 100 kHz to 0.01 Hz. The results of the EIS spectra were analyzed by using “ZSimpWin 3.10” software and fitted by the

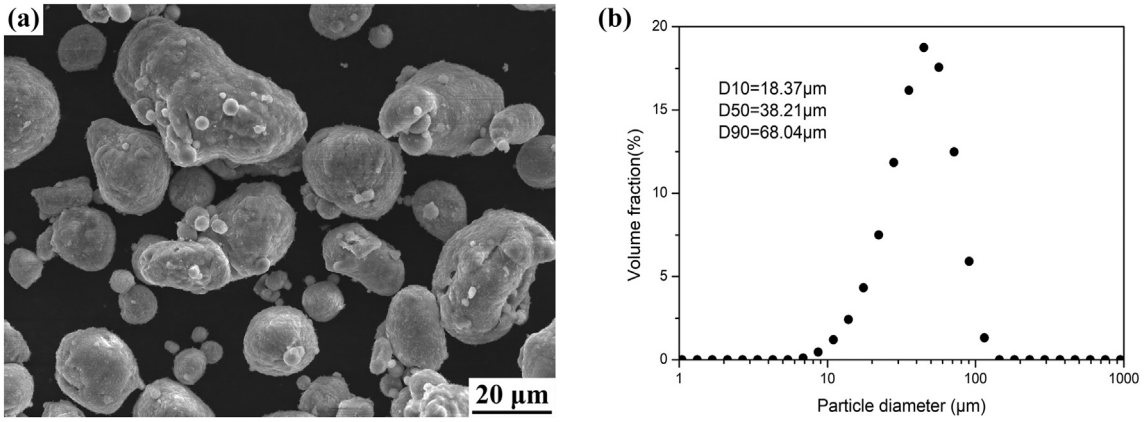

Fig. 1. Morphology (a) and size distributions (b) of Al powders.

appropriate equivalent circuits.

2.6. Long-term corrosion behavior

Neutral salt spray corrosion tests were performed on as-deposited pure Al-coated LA43M, shot-peened pure Al-coated LA43M alloy and bare LA43M alloy substrate. According to ASTM B117-16 standard, the samples were continuously exposed to 5 wt% NaCl salt spray at 35 °C for 1000 h in a Salt Fog Chamber (YWX/Q-250, Yashilin Testing Equipment CO., Ltd., Beijing, China) with a relative humidity of 100%. The pH value of the neutral salt spray is maintained 6.5–7.2. The salt fog in the chamber was collected regularly with a collector to ensure that the precipitation rate is within the range of 1.0–2.0 ml/80 cm^2·h. After different exposure times, three samples were taken out from the chamber and observed under SEM. The corrosion product was removed according to the ASTM G1-03 standard and weight of the samples was measured by an electronic weighing balance (0.1 mg).

A long-term immersion test in 3.5 wt% NaCl solution was carried out to obtain the EIS spectra of the pure Al-coated LA43M and shot peened Al coated LA43M alloy at different immersion time. The chemical composition and morphology of the corrosion layers formed on the specimen surfaces after 1000 h immersion tests were characterized by SEM and EDS.

3. Results and discussions

3.1. Microstructure and localized mechanical performance

Fig. 4 shows the surface morphology and cross-sectional microstructure of the cold sprayed Al coating. The surface morphology of pure Al coated LA43M and shot-peened pure Al coated LA43M were exhibited in Fig. 4a and b, respectively. Numerous incompletely deformed aluminum particles accumulated on the surface of pure Al coated LA43M, which creates lots of holes on the coating surface (Fig. 4a). These partially deformed particles disappeared after the shot peening process, leaved tamping marks of the shot peening particles and covered on the surface evenly. The cross-sectional microstructure of pure Al coated LA43M and shot-peened pure Al coated LA43M are presented in Fig. 4c and d, respectively. Fig. 4c exhibits a number of micron-sized pores and cracks between insufficient deformed particles, whereas a relatively dense microstructure has been observed in Fig. 4d after shot-peening. The porosity of the compact shot peened Al coating is only 0.2%, which is much lower than that of the traditional cold spraying coating of 12.4% and at the same level as in-situ shot peening [15,24]. The coating and substrate exhibited excellent interfacial adhesion after shot peening.

Fig. 4e shows the cross-sectional SEM image of the coating after being etched with sodium hydroxide (NaOH) solution at 70 °C for 5 s. In pure Al coated LA43M, some Al particles exhibited irregular spherical shape due to insufficient deformation results in the formation of pores. However, these pores completely vanished after shot peening as shown in Fig. 4f, where the original spherical Al particles become extremely flat. The flattening ratio corresponds to the degree of particle deformation due to shot peening treatment, which can be defined by using the average diameter of particles before and after impact [33]. The flattening ratio can also be used to estimate the deformation of deposited particles [31,34–36]. Herein, 20 particles are randomly selected from each sample to assess the flattening ratio. The flattening rate of as-deposited and shot-peened Al-coated LA43M alloys were found to be 1.46 and 3.47, respectively. Therefore, it can be concluded that the

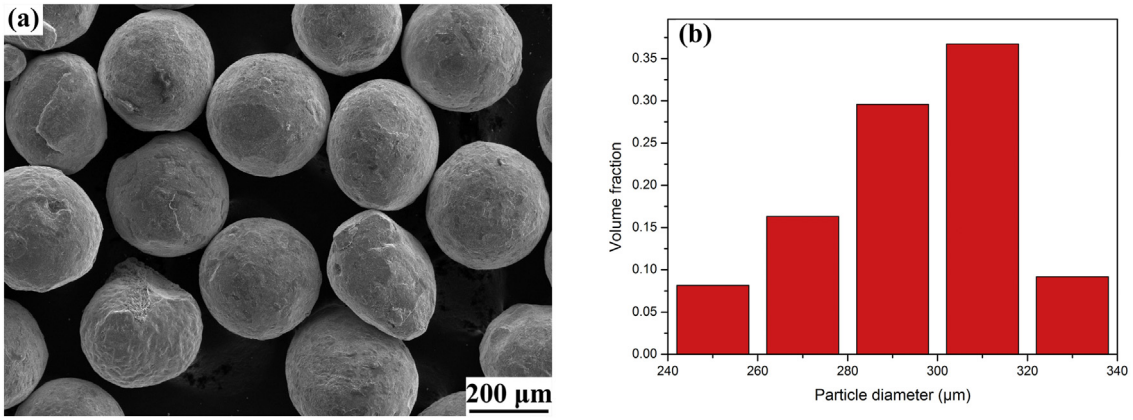

Fig. 2. Morphology (a) and size distributions (b) of the stainless steel shot peening particles.

Table 1
The composition of LA43M Mg–Li alloy, pure Al powders and bulk Al (wt%).

	Mg	Al	Li	Zn	Mn	Si	Fe	Cu	Cr
LA43M	Balance	2.5–3.5	3.5–4.5	2.5–3.5	/	0.50	0.05	0.05	/
Al powder	0.03	Balance	/	0.05	0.05	0.25	0.4	0.05	/
Bulk Al	0.02	Balance	/	0.05	0.03	0.25	0.3	0.05	0.01

Table 2
Cold spraying parameters of pure Al coating on LA43M substrate.

Gas	Gas temperature (°C)	Gas pressure (MPa)	Gun traverse speed (mm/s)	Standoff distance (mm)	Powder feeder rate (g/min)
N_2	280	3	40	20	35

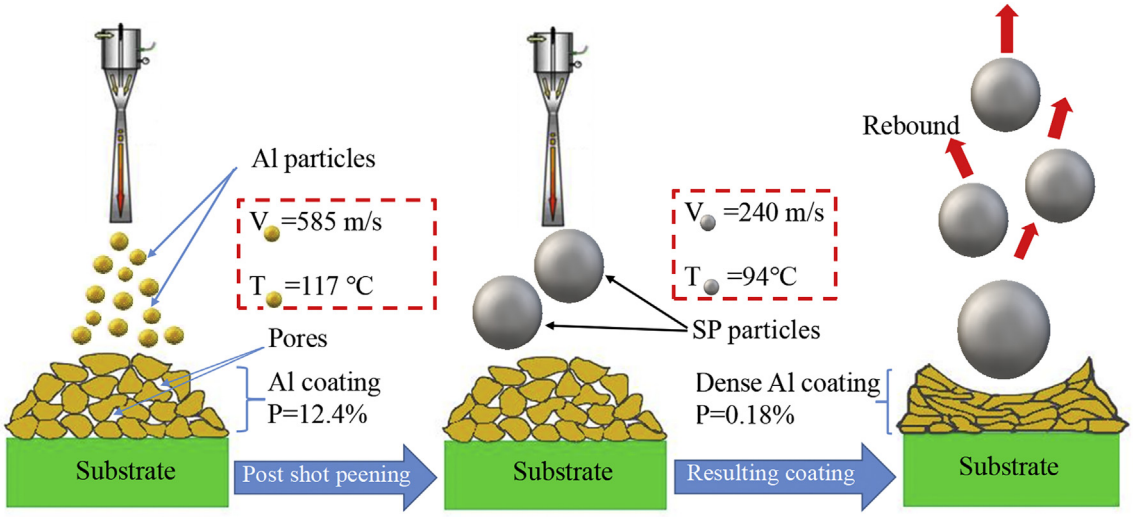

Fig. 3. The schematic illustration of cold spraying and shot peening processes to obtain dense Al coatings on LA43M substrates.

subsequent shot peening effectively enhanced the coating density.

The high-magnification SEM image of shot-peened pure Al coating in Fig. 4g shows the details of the bonding structure at coating/substrate interface. The interface is not showing any defect and Al particles are deeply embedded in the matrix, which confirms the excellent interfacial adhesion. It has also been reported that the cold sprayed coatings exhibit a reliable bonding with the substrate due to strong mechanical interlocking and metallurgical bonding [34,37,38]. The corresponding EDS analysis in Fig. 4h confirms the presence of an oxide-free interface between pure Al coating and substrate.

The micro-hardness profiles of pure Al coated LA43M and shot-peened pure Al coated LA43M across the interface are shown in Fig. 5. It can be clearly observed that the micro-hardness of pure Al coated LA43M decreased with increasing distance from the interface. However, due to the tamping effect of subsequent SS particles, the micro-hardness of shot-peened pure Al coated LA43M is increased on the near surface [39], which ascribed a severe change in internal microstructure and the decrease of coating porosity. It can be observed based on the trend of micro-hardness in Fig. 5 that the shot-peening affected coating depth is approximately 250 μm. During the post shot peening process, the pure Al coating can be severely impacted by heavy shot peening particles. This induced compressive stress on coating surface and enhanced micro-hardness, fatigue and wear properties of the coating [30,40]. The hardness of coating is improved by grain refinement and work hardening [15,24,27,41–43]. Therefore, post shot peening significantly enhanced the micro-hardness of cold spraying pure Al coating. In addition, the hardness of substrate is also increased as a result of grit blasting and cold spraying process.

3.2. Analysis of open circuit potential (OCP) and potentiodynamic polarization (PDP)

Fig. 6 shows the OCP curves of the bulk Al, LA43M substrate, pure Al coated LA43M and shot-peened pure Al coated LA43M specimens in a 3.5 wt% NaCl solution. The LA43M substrate has shown the lowest OCP of −1.62 V (V vs. SCE) after being immersed in the electrolyte solution for 1 h. The OCP of the pure Al-coated LA43M electrode has been significantly improved due to the presence of protective Al layer. The higher OCP corresponds to the enhanced corrosion resistance of the LA43M substrate. However, the cold spraying process results a porous coating due to insufficient deformation of the particles. Therefore, the electrolyte solution (3.5 wt% NaCl) permeates through the surface pores and reacts at the inter-particle boundaries, leading to a significant variation in OCP of pure Al coated LA43M [44]. On the other hand, the OCP value of shot-peened Al-coated LA43M electrode remained stable due to increased density of the coating. The OCP of shot-peened Al-coated LA43M (−0.8 V) is quite close to the OCP of bulk Al (−0.7 V), which indicates that shot peening process is critical to the compactness of the cold spraying Al coating.

The PDP curves of bulk Al, LA43M substrate, pure Al-coated LA43M and shot-peened Al-coated LA43M electrodes in 3.5 wt% NaCl solution after immersion for an hour is shown in Fig. 7. The corrosion potential (E_{corr}) and corrosion current density (I_{corr}) of different samples are summarized in Table 3. The corrosion potential value of the bare LA43M alloy is −1.51 V, which indicates the higher reactivity of LA43M substrate in 3.5 wt% NaCl solution. Whereas, the corrosion potential of pure Al-coated LA43M and shot-peened Al-coated LA43M electrodes increased to −0.92 V and −0.80 V, respectively. The

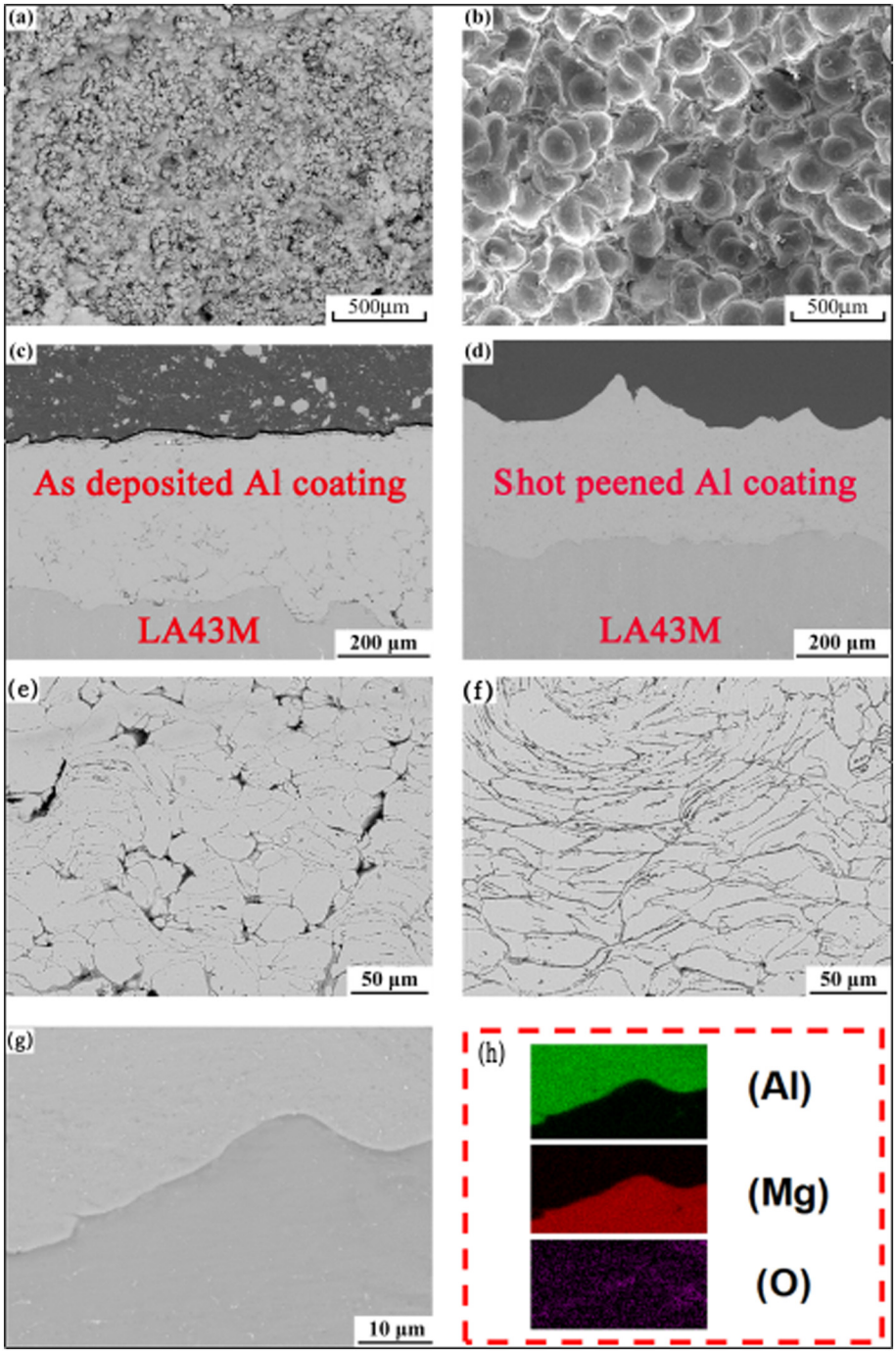

Fig. 4. Microstructural characterization: (a–b) surface morphology, (c–d) cross-sectional microstructure and (e–f) etched cross-sectional microstructure of pure Al coated LA43M and shot-peened pure Al coated LA43M, respectively. (g–h) a high-magnification SEM image of shot-peened Al coating and elemental distribution maps of coating/substrate interface.

significant increase in corrosion potential of pure Al-coated LA43M and shot-peened Al-coated LA43M electrodes indicates the enhanced corrosion resistance of Al-coated LA43M substrates in 3.5 wt% NaCl solution. However, the E_{corr} of the aluminum coating is higher than that of the LA43M substrate, which may result in severe galvanic corrosion if the corrosive media reach the substrate surface through the pores in the coating [45]. Therefore, the cold sprayed aluminum coating must be shot peened to increase the density. In addition, the corrosion current density reflects the overall corrosion rate on surface of different samples. The lower corrosion current density corresponds to the better corrosion resistance of the specimen [46]. The corrosion current density of pure Al-coated LA43M and shot-peened Al-coated LA43M electrodes is far lower than that of bare LA43M substrate. The shot-peened pure Al-coated LA43M electrode has shown a lower corrosion current density of 2.15×10^{-7} A·cm^{-2}, which is similar to the corrosion current density of bulk Al (1.48×10^{-7} A·cm^{-2}). The distinct difference between E_{corr} and I_{corr} of pure Al-coated LA43M and shot-peened pure Al-coated LA43M electrodes is due to the disappearance of the pores in the Al coating. The corrosion current density of shot-peened pure Al coating is comparable to the previously reported corrosion current density values of other coatings in a similar electrolyte [8,10,20,46–56]. Although some micro-arc oxidation coating and sealing composite coatings have lower corrosion current density than shot-peened pure Al coating, these organic sealing coatings are prone to failure in the long-term service

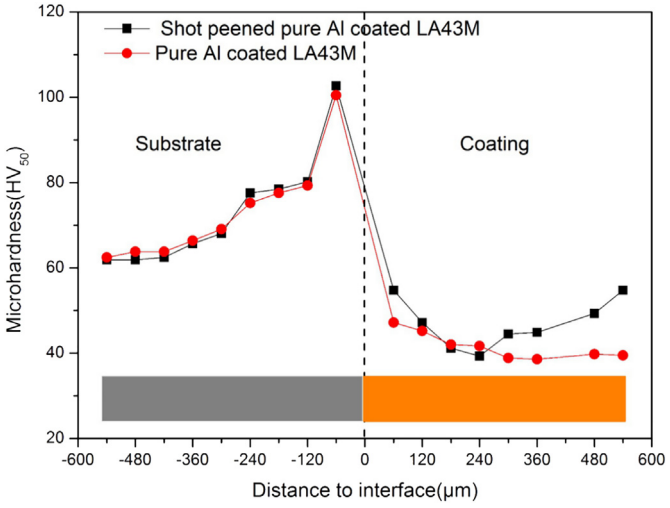

Fig. 5. Microhardness profiles of as-deposited and shot-peened Al coated LA43M coatings along the coating cross-section.

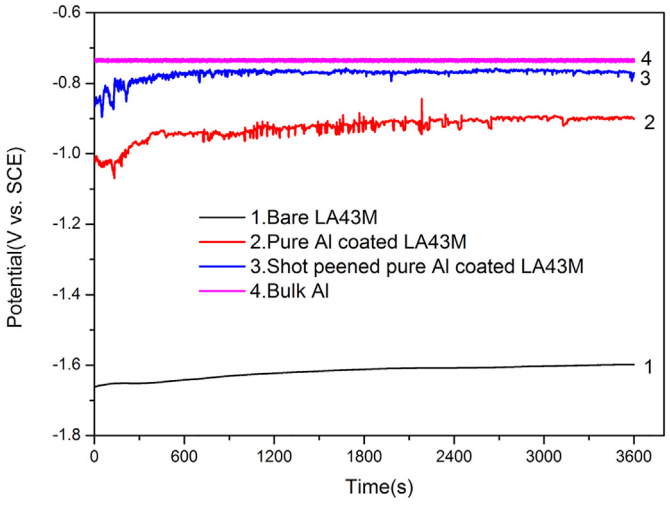

Fig. 6. OCP curves as a function of time for the bulk Al, bare LA43M, as-deposited pure Al coated LA43M and shot-peened pure Al coated LA43M specimens in 3.5 wt% NaCl solution.

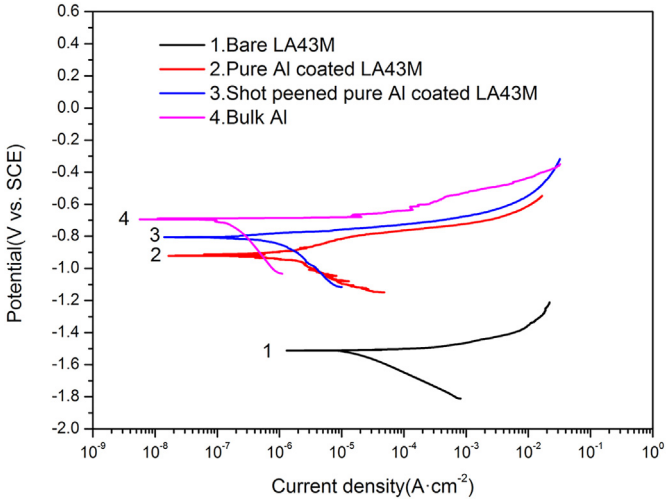

Fig. 7. Potentiodynamic polarization curves of the bulk Al, bare LA43M, as-deposited pure Al coated LA43M and shot peened pure Al coated LA43M specimens in 3.5 wt% NaCl solution.

Table 3
Potentiodynamic polarization and Tafel extrapolation results of as-deposited and shot-peened Al-coated LA43M substrates and their comparison with previously published results.

Samples	E_{corr} (V vs. SCE)	I_{corr} (A/cm^2)
Bare LA43M	−1.51	1.41E−5
Bulk Al	−0.70	1.48E−7
Pure Al coated LA43M	−0.92	2.97E−6
Shot peened pure Al coated LA43M	−0.80	2.15E−7
Ni coating AZ31B [46]	−0.29	7.30E−7
Al-50 coating on AZ91D [20]	−0.91	3.40E−6
MAO coatings on AZ31 [47]	−1.41	2.86E−8
MAO with activation/Ni–P (2 min) [48]	−0.78	4.79E−9
PANI-PhA/silane coating [49]	−1.46	1.28E−7
Phenolic conversion coating [50]	−1.62	8.09E−7
Annealed MAO coatings(250 °C) [51]	−0.54	2.96E−7
Ag/HA composite conversion coating [52]	−1.41	4.11E−6
AZ91D + MAO + G502 + Ni [53]	−0.351	3.12E−7
FHAp3/MAO coating [8]	−1.51	3.87E−7
Ca-P-Sn coating on Mg-1Li-1Ca [54]	−1.47	1.87E−6
rGO 0.1/Apatite coating on AZ31B [55]	−1.38	3.35E−5
Double layer Ni/Ni-B coating [10]	−0.47	1.10E−7
Ni-LDH/MAO coating on AZ31 [56]	–	3.20E−7

environment [57]. Compared with different sealing methods, such as solution processing, electroplating and heat treatment [48,51,58], the subsequent shot peening treatment is a simple, cost-effective and eco-friendly process. Therefore, shot peening treatment is an efficient method to enhance the corrosion resistance of cold spraying Al-coated LA43M substrate.

3.3. Electrochemical impedance spectroscopy (EIS) analysis

To elucidate the protective effect of pure aluminum coating on LA43M alloy more accurately, the electrochemical impedance spectroscopy (EIS) were collected at OCP after being immersed in 3.5 wt% NaCl solution for 2 h. Fig. 8 presents the Nyquist and Bode plot results of the LA43M substrate, as-deposited Al-coated LA43M and shot-peened Al-coated LA43M electrodes. In the case of LA43M substrate, the Nyquist plot shows two capacitive loops in the high-frequency region and medium-frequency. It also presents an inductive loop in the low-frequency region (Fig. 8b), which are consistent with the previously published literatures [2,59]. The porous oxide films on LA43M alloy only play a small role in blocking the corrosion solution, resulting in an impedance response in medium-frequency is not very obvious [60–62]. The high-frequency capacitive loop corresponds to the charge transfer resistance due to electrical double layer effect. The presence of the low-frequency inductive loop is due to the dissolution of the passivation film and pitting corrosion [4,57,63,64], and small capacitive loop indicates the poor corrosion resistance of LA43M substrate [65]. The as-deposited Al-coated LA43M alloy exhibited two capacitive loops and did not show any inductive loop [66]. Fig. 8a shows that the diameter of the capacitive loop of as-deposited Al-coated LA43M alloy is remarkably larger than that of LA43M substrate, which indicates the higher corrosion resistance due to the presence of Al coating. The charge transfer resistance of the electrochemical reaction, corresponding to the diameter of the capacitive loop which is increased due to shot peening treatment. This implies that the shot-peened Al-coated LA43M alloy exhibits highest corrosion resistance among three studied samples. According to previous investigation, the low-frequency impedance (|Z|) value is related to the corrosion resistance [67,68]. The increase in the low-frequency impedance (|Z|) value after shot peening indicates an enhancement in corrosion resistance, as shown in Fig. 8c. Fig. 8d present the phase diagram of bare LA43M, as-deposited Al-coated LA43M and shot-peened Al-coated LA43M alloys. The phase angle of shot-peened Al-coated LA43M maintained a higher value over a wide range of intermediate frequencies, indicating the uniform and

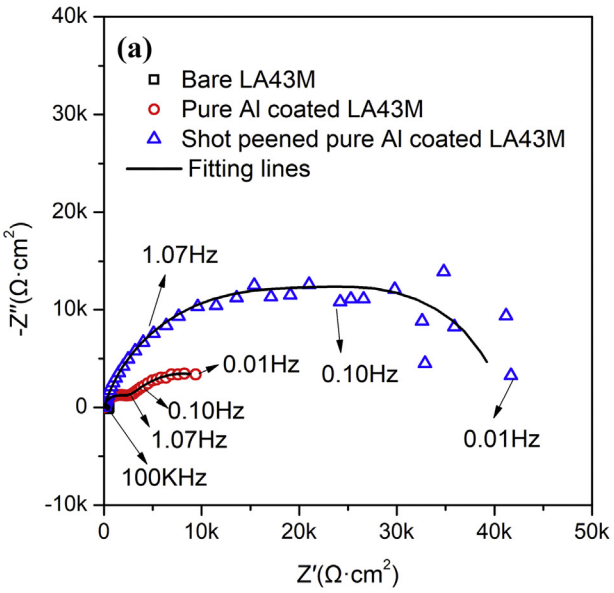

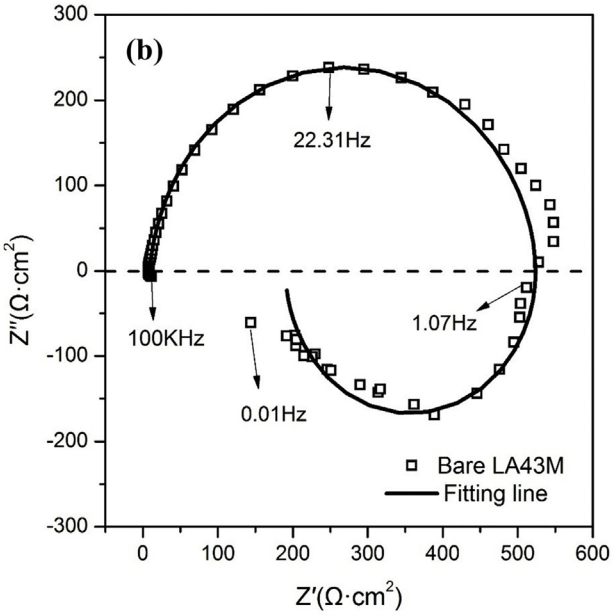

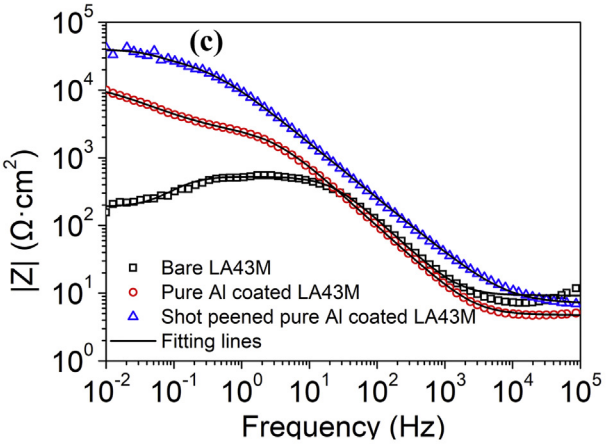

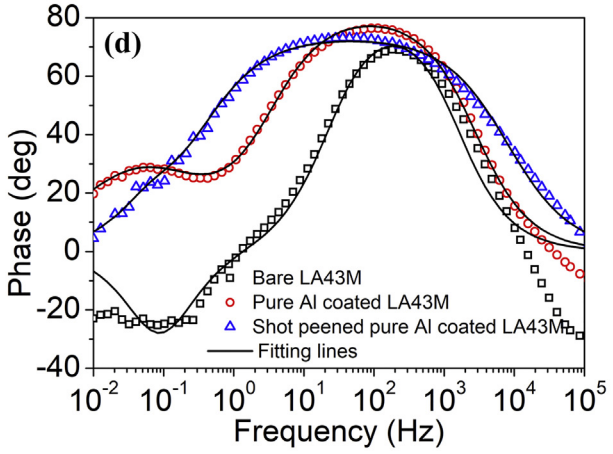

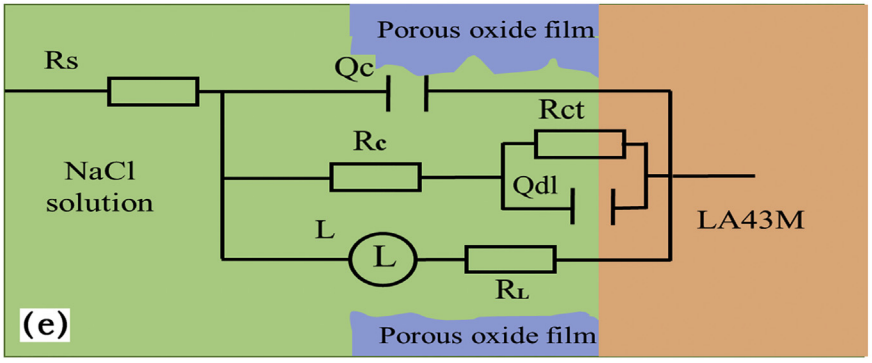

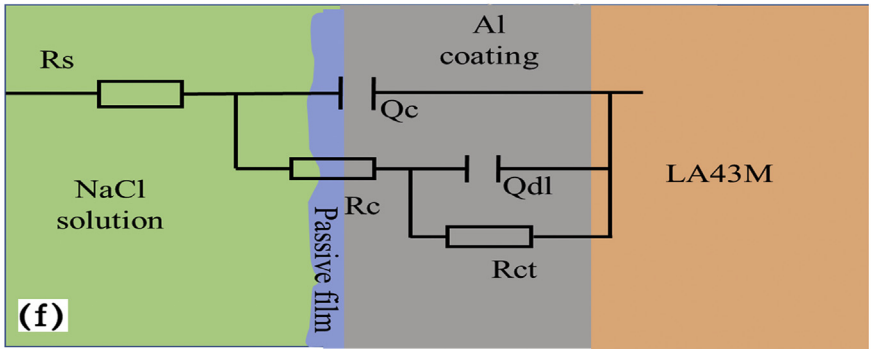

(caption on next page)

Fig. 8. EIS spectra and fitting results of bare LA43M, as-deposited Al-coated LA43M and shot-peened Al-coated LA43M alloy after being immersed in 3.5 wt% NaCl solution for 2 h. (a, b) Nyquist plots and (c, d) Bode plots. The equivalent circuits for EIS data fitting: (e) bare LA43M alloy and (f) Al-coated LA43M alloys.

Table 4
Electrochemical data obtained via equivalent circuit fitting of the EIS curves for the samples in 3.5 wt% NaCl solution.

Sample	Bare LA43M	As-deposited Al-coated LA43M	Shot-peened Al-coated LA43M
Rs (Ω·cm^2)	9.23	4.75	7.01
Q_c (S sn/cm^2)	1.07×10^{-5}	2.88×10^{-5}	2.04×10^{-5}
n_1	0.98	0.91	0.82
R_c (Ω·cm^2)	168.10	2.52×10^{3}	5.09×10^{4}
Q_{dl} (S s_n/cm^2)	2.36×10^{-5}	4.6×10^{-4}	2.45×10^{-4}
n_2	0.82	0.80	0.93
R_{ct} (Ω·cm^2)	358.4	1.16×10^{4}	2.11×10^{4}
R_L (Ω·cm^2)	278.4	–	–
L (H cm^2)	842.5	–	–

dense nature of the shot peened pure Al coating [57,69].

The equivalent circuit diagrams of bare LA43M and Al-coated LA43M alloys are presented in Fig. 8e and f, respectively. The EIS spectrum of bare LA43M alloy can be fitted by using $R_s(Q_c(R_c(Q_{dl}R_{ct})(R_LL))$ model, where R_s refers to the solution resistance. R_c represents the resistance of the porous oxide film and Q_c is the capacitance. For LA43M alloy, the porous oxide film on the surface is very thin and it is broken down easily after immersion in 3.5 wt% NaCl solution for a short time [11]. The R_c value of only 168.10 Ω·cm^2 in the fitting of the impedance spectrum was obtained. Therefore, the oxide film only plays a small role in blocking the corrosion solution. R_{ct} represents charge transfer resistance and Q_{dl} corresponds to the electrical double layer capacitance, which represents the redox process that occurs at the interface between the porous oxide film and the LA43M substrate. R_L and L represent the low-frequency resistance and inductance, respectively. Song et al. have indicated that alloying of lithium can deteriorate the

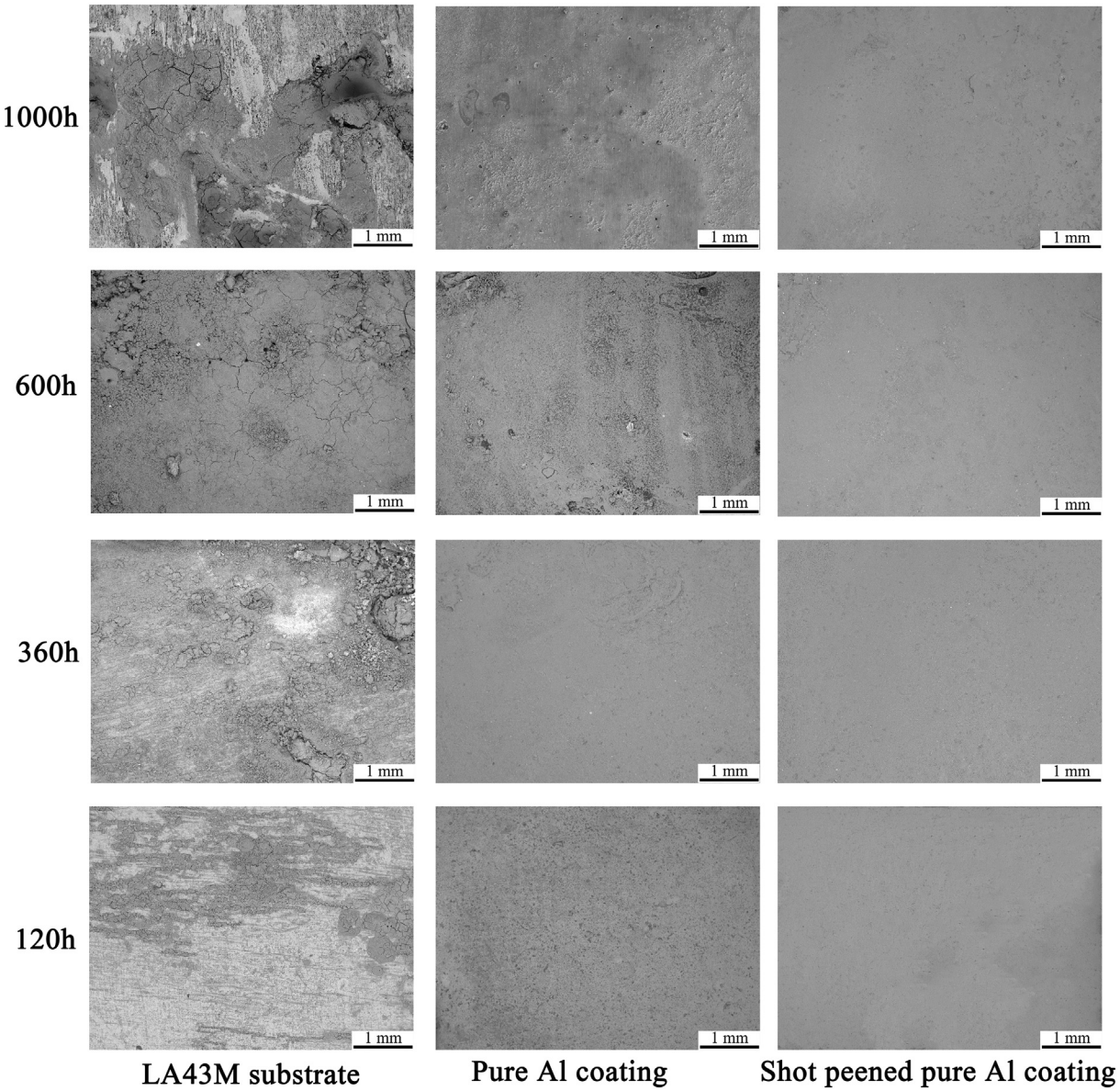

Fig. 9. Surface morphology of the bare LA43M alloy, as-deposited pure Al coated LA43M and shot-peened Al coated LA43M substrates after being exposed to 5 wt% NaCl neutral salt spray for 120, 360, 600, and 1000 h.

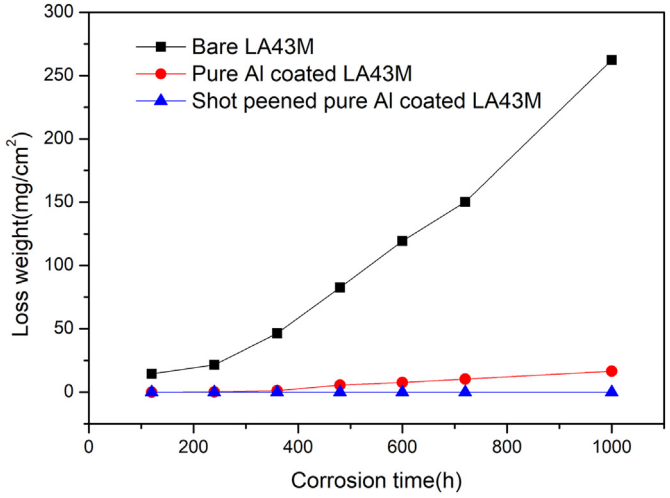

Fig. 10. Loss weight of bare LA43M, as-deposited pure Al coated LA43M and shot-peened Al-coated LA43M alloys in 5 wt% NaCl neutral salt spray as a function of exposure time.

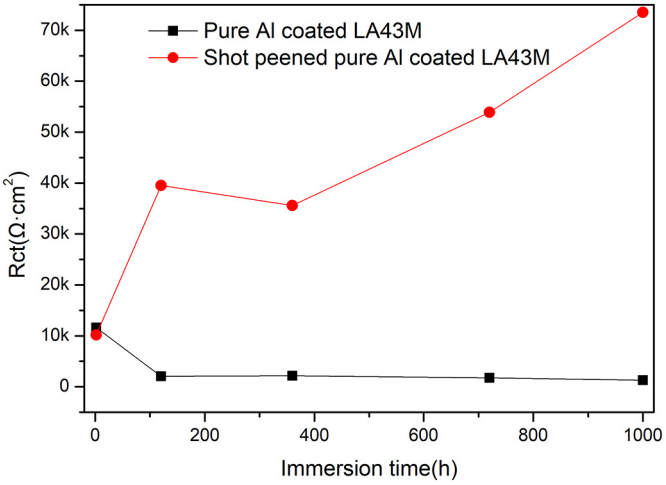

Fig. 12. The evolution of charge transfer resistance after different immersed periods in 3.5 wt% NaCl solutions.

corrosion resistance of magnesium substrate [4]. So, the corrosion resistance of Mg—Li alloy is worse than that of ordinary magnesium alloy. The corrosion nucleation at the initiation stage of localized corrosion on the LA43M substrate result the low frequency inductive loop extended to a large frequency scanning scale.

For the equivalent circuit of specimens protected by aluminum coating as shown in Fig. 8f, R_s is the solution resistance. Q_c is the capacitance and R_c represents the resistance of the Al coating [70]. Q_{dl} and R_{ct} refer to the electrical double layer capacitance and charge transfer resistance, respectively. Thus, the model can be expressed as $R_s(Q_c(R_c(Q_{dl}R_{ct})))$. The EIS fitting results of the two coatings and LA43M substrate are summarized in Table 4. It can be found that the R_{ct} value of as-deposited Al-coated LA43M alloy increased from 358.4 Ω·cm^2 to 1.16 × 10^4 Ω·cm^2 compared with LA43M substrate. Furthermore, the R_c value of shot-peened Al-coated LA43M alloy is higher than the as-deposited Al-coated LA43M alloy, which can be attributed to dense coating after shot peening treatment.

3.4. Neutral salt spray corrosion analysis

The corrosion morphologies of bare LA43M alloy, as deposited pure Al coated LA43M and shot-peened pure Al coated LA43M substrates, after being exposed to 5 wt% NaCl neutral salt spray for 120 h, 360 h, 600 h and 1000 h, are shown in Fig. 9. The filiform corrosion occurred on the surface of bare LA43M alloy after being exposed to neutral salt spray for 120 h. With the increase of exposure time, the corrosion pits and cracks started appearing and loose corrosion products covered the surface of bare LA43M substrate. For the pure Al coated LA43M samples, there were no significant corrosion occurred at the beginning. However, pitting occurred obviously on the surface of the sample after 600 h of salt spray. With the increase in salt spray time, the pitting density increases with uniform corrosion. This is similar to the reported morphology of the corrosion of aluminum [57,71]. Due to the compactness of the aluminum coating after shot peening, the corrosion solution cannot enter the interior of the coating. In addition, shot peening process introduces compressive stress to the surface of the coating, which further enhanced the corrosion resistance of the coating [26–29]. Therefore, the surface of shot peened Al-coated LA43M remained smooth and almost no traces of corrosion can be seen after being exposed to neutral salt spray for 1000 h. Weight loss of three

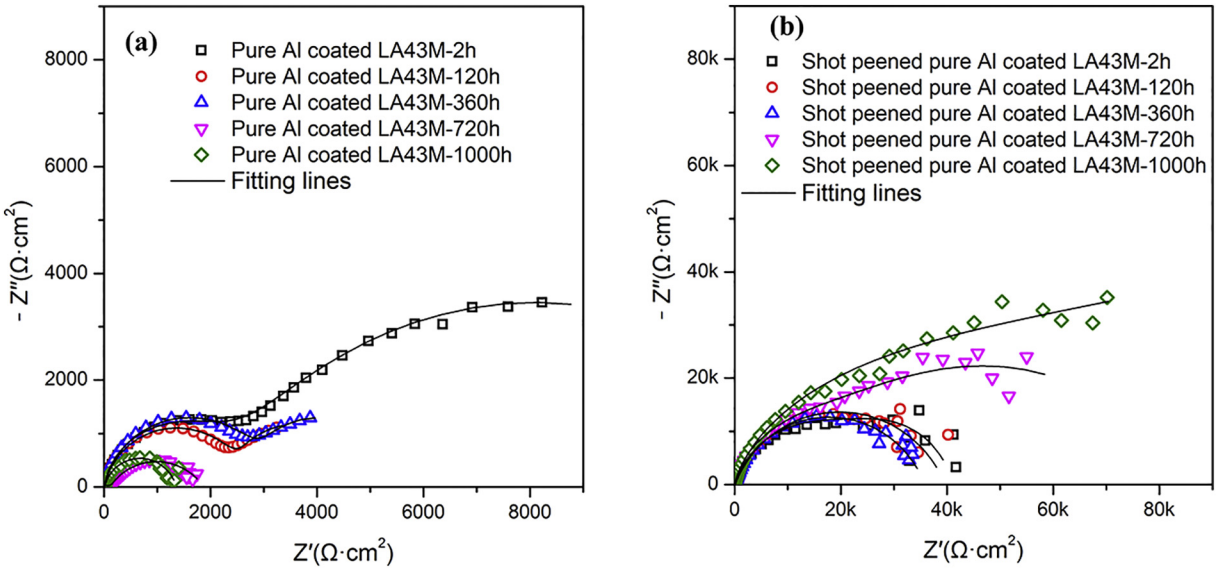

Fig. 11. The Nyquist plots (a) as-deposited pure Al coated LA43M (b) shot peened pure Al coated LA43M after different immersed periods in 3.5 wt% NaCl solutions.

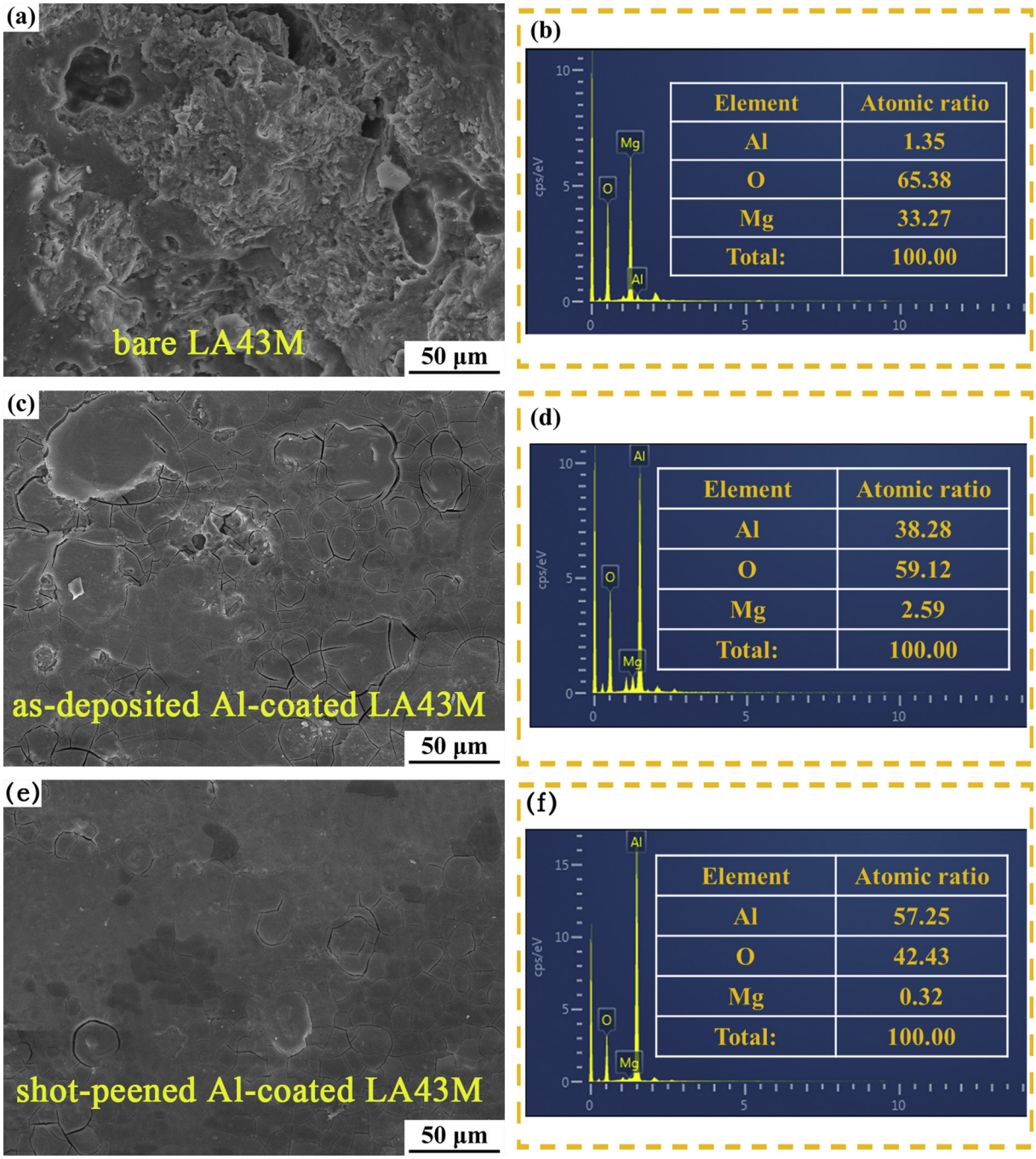

Fig. 13. The chemical composition and morphology of the corrosion layers formed on the specimen surfaces after 1000 h immersion tests. (a, b) bare LA43M, (c, d) as-deposited Al-coated LA43M and (e, f) shot-peened Al-coated LA43M.

types of samples after different exposure times are presented in Fig. 10. In the case of LA43M substrate, the weight loss linearly increased with exposure time and attained a value of 262.5 mg/cm^2 after 1000 h salt spray corrosion. This indicates that the corrosion products are porous and do not protect the further corrosion of LA43M substrate. For specimens protected by pure Al coating, the weight loss results are completely different from the substrate. The value of weight loss for pure Al coated LA43M during 1000 h salt spray increased slightly because the coating structure is not dense. On the other hand, the weight loss of shot-peened Al-coated LA43M substrate can be ignored, indicating the long-term corrosion resistance of shot-peened Al-coated LA43M alloy in a neutral salt environment.

3.5. Long-term immersion corrosion behavior

To further study the effect of shot peening on the corrosion resistance of samples during the long-term immersion. Fig. 11 shows the Nyquist plots of as-deposited Al-coated LA43M and shot peened pure Al coated LA43M at various immersion periods. The fitting lines are plotted according to equivalent circuit shown in Fig. 8f. It can be found that the diameter of the capacitive loop for pure Al coated LA43M alloy in Fig. 11a decreased with immersion time from 2 h to 1000 h. It is noted that the semicircle diameter increased slightly at 360 h, which is attributed to the formation of aluminum oxide film on the surface of the pure Al coating [72]. However, the oxide film is not dense due to the defects of the coating itself. So, the diameter of the capacitive loop

decreased again after 720 h immersion. The capacitive loop for shot peened pure Al coated LA43M in Fig. 11b did not decrease during the 1000 h immersion, which indicated the significant effect of shot peening on densification of pure aluminum coatings. Moreover, the semicircle diameter gradually increases with the extension of the immersion time because a good coverage Al_2O_3 film was formed on the dense aluminum coating surface [70,72].

The evolution of charge transfer resistance during immersion is presented in Fig. 12. The as-deposited pure Al coating cannot effectively block the corrosion solution due to the presence of pores inside it. Therefore, after 1000 h of immersion, the charge transfer resistance decreased to 1248 $\Omega{\cdot}cm^2$ and the corrosion resistance of the coating was greatly reduced. For the shot peened pure Al coated LA43M, the surface of the aluminum coating is dense and the alumina film formed during the immersion process has fewer defects. So, the charge transfer resistance is significantly greater than the coating before shot peening. It can be found that the charge transfer resistance increased to 73,500 $\Omega{\cdot}cm^2$ after 1000 h immersion, which is more than three times the initial value. This indicates the relatively alumina film further improves the corrosion resistance of the coating. Hence, shot peening process is an effective method to eliminate coating porosity and significantly improve coating corrosion resistance for a long term.

The chemical composition and morphology of the corrosion layers formed on the specimen surfaces after 1000 h immersion tests have been characterized by SEM and EDS in Fig. 13. The LA43M substrate displayed the typical corrosion characteristics of magnesium alloys as shown in Fig. 13a and b, indicating that the corrosion products mainly included Mg hydroxide and Mg oxide [62,73]. The results for the as-deposited Al-coated LA43M are shown in Fig. 13c and d. In terms of morphology, the surface of the specimen without shot peening was mostly covered by corrosion pits and cracks. The predominant elements are Al and O, implying that the both corrosion products are mainly alumina [16,74]. The oxygen content of the coatings before shot peening is significantly higher than the coating after shot peening, which is because further oxidation occurred when the solution entered the coating through pores. Whereas, the dense shot peened pure Al coating effectively prevented further oxidation and the results are shown in Fig. 13e and f. After the shot peening process, there were only a few cracks on the surface, which showed that the shot peened pure Al coating safeguarded the substrate for a long time.

4. Conclusions

Conventional cold spraying and shot peening treatment were used to obtain dense Al coatings on LA43M substrate and the influence of shot peening treatment on the corrosion resistance of cold-sprayed Al coatings has been systematically studied. After being tamped by subsequent stainless-steel shot peening, the kinetic energy of martensitic stainless-steel particles has been absorbed by Al particles, resulted in a significantly higher fraction of flattened Al particles. The shot-peened Al coating has shown an extremely lower porosity of only 0.2% than conventional cold-sprayed Al coating (12.4%). Furthermore, the shot-peened Al-coated LA43M sample has exhibited a higher open circuit potential, lower corrosion current density and better impedance values than the as-deposited Al-coated LA43M sample. The salt spray corrosion morphology shows that the shot-peened Al coating can effectively protect the LA43M substrate from corrosion under severe conditions. Surface energy spectrum analysis and impedance behavior of the samples during long term immersion indicate that the shot peening process plays a critical role on the compactness of the pure Al coating and greatly improves the protective effect of the pure Al coating on the LA43M substrate.

CRediT authorship contribution statement

Fei-Fei Lu: Data curation, Writing - review & editing, Methodology.**Kai Ma:**Visualization, Investigation.**Cheng-Xin Li:**Supervision.**Muhammad Yasir:**Conceptualization.**Xiao-Tao Luo:**Software, Formal analysis.**Chang-jiu Li:**Resources.

Declaration of competing interest

We declare that we have no financial and personal relationships with other people or organizations that can inappropriately influence our work. There is no professional or other personal interest of any nature or kind in any product, service or company that could be construed as influencing the position presented in, or the review of, the manuscript entitled “Enhanced corrosion resistance of cold-sprayed and shot-peened aluminum coatings on LA43M magnesium alloy”.

Acknowledgements

The authors would like to thank the National Science Foundation of China for financial support (No. 51761145108).

Data availability

The raw/processed data required to reproduce these findings cannot be shared at this time due to technical or time limitations.

References

[1] H. Yue Sun, C. Ri Wang, Q. Chao Peng, Yan Feng, Ming Yang, Corrosion Behavior and Surface Treatment of Superlight Mg–Li Alloys.
[2] C.Q. Li, D.K. Xu, X.B. Chen, B.J. Wang, R.Z. Wu, E.H. Han, N. Birbilis, Composition and microstructure dependent corrosion behaviour of Mg-Li alloys, Electrochim. Acta 260 (2018) 55–64.
[3] M. Esmaily, J.E. Svensson, S. Fajardo, N. Birbilis, G.S. Frankel, S. Virtanen, R. Arrabal, S. Thomas, L.G. Johansson, Fundamentals and advances in magnesium alloy corrosion, Prog. Mater. Sci. 89 (2017) 92–193.
[4] Y. Song, D. Shan, R. Chen, E.-H. Han, Corrosion characterization of Mg–8Li alloy in NaCl solution, Corros. Sci. 51 (2009) 1087–1094.
[5] A. Atrens, G.-L. Song, M. Liu, Z. Shi, F. Cao, M.S. Dargusch, Review of recent developments in the field of magnesium corrosion, Adv. Eng. Mater. 17 (2015) 400–453.
[6] G.-R. Li, L.-S. Wang, W.-W. Zhang, G.-J. Yang, X.-F. Chen, W.-X. Zhang, Tailoring degradation-resistant thermal barrier coatings based on the orientation of spontaneously formed pores: from retardation to self-improvement, Compos. Part B 181 (2020) 107567.
[7] Y. Wang, Z. Gu, J. Liu, J. Jiang, N. Yuan, J. Pu, J. Ding, An organic/inorganic composite multi-layer coating to improve the corrosion resistance of AZ31B Mg alloy, Surf. Coat. Technol. 360 (2019) 276–284.
[8] Wentao Yu, Ruixue Sun, Ziqiang Guo, Zhiyuan Wang, Yong He, Guangyi Lu, Panyu Chen, K. Chen, Novel fluoridated hydroxyapatite_MAO composite coating on AZ31B magnesium alloy for biomedical application, Appl. Surf. Sci. 464 (2019) 708–715.
[9] A. Francis, Y. Yang, A.R. Boccaccini, A new strategy for developing chitosan conversion coating on magnesium substrates for orthopedic implants, Appl. Surf. Sci. 466 (2019) 854–862.
[10] C. Hu, M. Xu, J. Zhang, B. Hu, G. Yu, High corrosion resistance of electroless Ni/Ni-B coating from fluoride-free baths on AZ31 magnesium alloy, J. Alloys Compd. 770 (2019) 48–57.
[11] Y.-h. Sun, R.-c. Wang, C.-q. Peng, Y. Feng, M. Yang, Corrosion behavior and surface treatment of superlight Mg–Li alloys, Trans. Nonferrous Metals Soc. China 27 (2017) 1455–1475.
[12] H. Assadi, H. Kreye, F. Gärtner, T. Klassen, Cold spraying – a materials perspective, Acta Mater. 116 (2016) 382–407.
[13] M.R. Rokni, S.R. Nutt, C.A. Widener, V.K. Champagne, R.H. Hrabe, Review of relationship between particle deformation, coating microstructure, and properties in high-pressure cold spray, J. Therm. Spray Technol. 26 (2017) 1308–1355.
[14] Y. Liu, C.-x. Li, X.-F. Huang, K. Ma, X.-T. Luo, C.-j. Li, Effect of water environment on particle deposition of underwater cold spray, Appl. Surf. Sci. 506 (2020) 144542.
[15] S.L. Fu, C.-X. Li, Y.-K. Wei, X.-T. Luo, G.-J. Yang, C.-J. Li, J.-L. Li, Novel method of aluminum to copper bonding by cold spray, J. Therm. Spray Technol..
[16] M. Trueba, P.T. Stefano, Study of Al alloy corrosion in neutral NaCl by the pitting scan technique, Materials Chemistry & Physics, 121 523–533.
[17] M. Diab, X. Pang, H. Jahed, The effect of pure aluminum cold spray coating on corrosion and corrosion fatigue of magnesium (3% Al-1% Zn) extrusion, Surf. Coat. Technol. 309 (2017) 423–435.
[18] C.J. Li, L. Wen-Ya, Deposition characteristics of titanium coating in cold spraying, Surface & Coatings Technology, 167 278–283.
[19] R. Fernandez, B. Jodoin, Cold spray aluminum–alumina cermet coatings: effect of alumina content, J. Therm. Spray Technol. 27 (2018) 603–623.

[20] H. Bu, M. Yandouzi, C. Lu, D. MacDonald, B. Jodoin, Cold spray blended Al +$Mg_{17}Al_{12}$ coating for corrosion protection of AZ91D magnesium alloy, Surf. Coat. Technol. 207 (2012) 155–162.

[21] B.S. Deforce, J.E. Timothy, K.P. John, Cold Spray Al-5% Mg Coatings for the Corrosion Protection of Magnesium Alloys, 20 1352–1358.

[22] M. Yu, H. Chen, W.Y. Li, Building-Up Process of Cold-Sprayed Al5056/In718 Composite Coating[J]. Therm. Spray Technol. 24 (2015) 579–586.

[23] E. Irissou, J.-G. Legoux, B. Arsenault, C. Moreau, Investigation of Al-Al_2O_3 cold spray coating formation and properties, J. Therm. Spray Technol. 16 (2007) 661–668.

[24] Y.-K. Wei, X.-T. Luo, C.-X. Li, C.-J. Li, Optimization of in-situ shot-peening-assisted cold spraying parameters for full corrosion protection of Mg alloy by fully dense Al-based alloy coating, J. Therm. Spray Technol. 26 (2016) 173–183.

[25] H. Zhou, C. Li, G. Ji, S. Fu, H. Yang, X. Luo, G. Yang, C. Li, Local microstructure inhomogeneity and gas temperature effect in in-situ shot-peening assisted cold-sprayed Ti-6Al-4V coating, J. Alloys Compd. 766 (2018) 694–704.

[26] A. Moridi, S.M. Hassani-Gangaraj, S. Vezzú, L. Trško, M. Guagliano, Fatigue behavior of cold spray coatings: the effect of conventional and severe shot peening as pre-/post-treatment, Surface & Coatings Technology 283 (2015) 247–254.

[27] A. Avilés, R. Avilés, J. Albizuri, L. Pallarés-Santasmartas, A. Rodríguez, Effect of shot-peening and low-plasticity burnishing on the high-cycle fatigue strength of DIN 34CrNiMo6 alloy steel, Int. J. Fatigue 119 (2019) 338–354.

[28] K. Zhu, Z. Li, C. Jiang, Surface mechanical properties of shot-peened CNT_Al-Mg-Si alloy composites, J. Alloys Compd. 773 (2019) 1048–1053.

[29] K.A. Habi, D.L. Cano, José Antonio Heredia, J.S. Mira, Effect of post-coating technique on microstructure, microhardness and the mixed lubrication regime parameters of thermally-sprayed NiCrBSi coatings, Surface & Coatings Technology 358 (2019) 824–832.

[30] Cancan Liu, Hui Zheng, Xin Gu, Bailing Jiang, Jun Liang, Effect of severe shot peening on corrosion behavior of AZ31 and AZ91 magnesium alloys, J. Alloys Compd. 770 (2019) 500–506.

[31] Jingwei Wu, H. Fang, H. Kim, C. Lee, High speed impact behaviors of Al alloy particle onto mild steel substrate during kinetic deposition, Mater. Sci. Eng. 417 (2006) 114–119.

[32] J.-J. Tian, Y.-K. Wei, C.-X. Li, G.-J. Yang, C.-J. Li, Effect of post-spray shot peening treatment on the corrosion behavior of NiCr-Mo coating by plasma spraying of the shell–core–structured powders, J. Therm. Spray Technol. 27 (2017) 232–242.

[33] E. Sansoucy, P. Marcoux, L. Ajdelsztajn, Properties of SiC-reinforced aluminum alloy coatings produced by the cold gas dynamic spraying process[J], Surf. Coat. Technol. 202 (2008) 3988–3996.

[34] P. Nautiyal, C. Zhang, V.K. Champagne, B. Boesl, A. Agarwal, In-situ mechanical investigation of the deformation of splat interfaces in cold-sprayed aluminum alloy, Mater. Sci. Eng. A 737 (2018) 297–309.

[35] Kicheol Kang, Sanghoon Yoon, Youlgwun Ji, C. Lee, Oxidation dependency of critical velocity for aluminum feedstock deposition in kinetic spraying process, Mater. Sci. Eng. A 486 (2008) 300–307.

[36] H. Assadi, F. Gartner, T. Stoltenhoff, H. Kreye, Bonding mechanism in cold gas spraying, Acta Mater. 51 (2003) 4379–4394.

[37] V.K. Champagne, D. Helfritch, P. Leyman, S. Grendahl, B. Klotz, Interface material mixing formed by the deposition of copper on aluminum by means of the cold spray process, J. Therm. Spray Technol. 14 (2005) 330–334.

[38] J.O.C.n. K.H. Ko, H. Lee, The interfacial restructuring to amorphous: a new adhesion mechanism of cold-sprayed coatings, Mater. Lett..

[39] X.-T. Luo, Y.-K. Wei, Y. Wang, C.-J. Li, Microstructure and mechanical property of Ti and Ti6Al4V prepared by an in-situ shot peening assisted cold spraying, Mater. Des. 85 (2015) 527–533.

[40] K. Wu, Y.Q. Wang, M.Y. Zheng, Effects of microarc oxidation surface treatment on the mechanical properties of Mg alloy and Mg matrix composites, Materials Science & Engineering A, 447 227–232.

[41] Y. Zou, W. Qin, E. Irissou, J.-G. Legoux, S. Yue, J.A. Szpunar, Dynamic recrystallization in the particle/particle interfacial region of cold-sprayed nickel coating: electron backscatter diffraction characterization, Scr. Mater. 61 (2009) 899–902.

[42] L. Tan, X. Ren, K. Sridharan, T.R. Allen, Effect of shot-peening on the oxidation of alloy 800H exposed to supercritical water and cyclic oxidation, Corros. Sci. 50 (2008) 2040–2046.

[43] R. Saillard, B. Viguier, G. Odemer, A. Pugliara, B. Fori, C. Blanc, Influence of the microstructure on the corrosion behaviour of 2024 aluminium alloy coated with a trivalent chromium conversion layer, Corros. Sci. 142 (2018) 119–132.

[44] D. Dzhurinskiy, E. Maeva, E. Leshchinsky, R.G. Maev, Corrosion protection of light alloys using low pressure cold spray, J. Therm. Spray Technol. 21 (2012) 304–313.

[45] K. Spencer, D.M. Fabijanic, M.X. Zhang, The use of Al–Al_2O_3 cold spray coatings to improve the surface properties of magnesium alloys, Surf. Coat. Technol. 204 (2009) 336–344.

[46] Y.-K. Wei, Y.-J. Li, Y. Zhang, X.-T. Luo, C.-J. Li, Corrosion resistant nickel coating with strong adhesion on AZ31B magnesium alloy prepared by an in-situ shot-peening-assisted cold spray, Corros. Sci. 138 (2018) 105–115.

[47] A. Keyvani, M. Zamani, A. Fattah-Alhosseini, S.H. Nourbakhsh, M. Bahamirian, Microstructure and corrosion resistance of MAO coatings on AZ31 magnesium, Materials Research Express 5 (2018) 086510.

[48] S.-Y. Jian, J.-L. Lee, H.-B. Lee, H.-H. Sheu, C.-Y. Ou, M.-D. Ger, Influence of electroless plating on the deterioration of the corrosion resistance of MAO coated AZ31B magnesium alloy, J. Taiwan Inst. Chem. Eng. 68 (2016) 496–505.

[49] X. Gao, X. Jing, Y. Li, J. Zhu, M. Zhang, Synthesis and characterization of phosphorized polyaniline doped with phytic acid and its anticorrosion properties for Mg-Li alloy, J. Macromol. Sci. A 55 (2017) 24–35.

[50] S. Chen, S. Zhao, M. Chen, X. Zhang, J. Zhang, X. Li, H. Zhang, X. Shen, J. Wang, N. Huang, The anticorrosion mechanism of phenolic conversion coating applied on magnesium implants, Appl. Surf. Sci. 463 (2019) 953–967.

[51] Z. Xu, U. Eduok, J. Szpunar, Effect of annealing temperature on the corrosion resistance of MgO coatings on Mg alloy, Surf. Coat. Technol. 357 (2019) 691–697.

[52] G. Hu, L. Zeng, H. Du, X. Fu, X. Jin, M. Deng, Y. Zhao, X. Liu, The formation mechanism and bio-corrosion properties of Ag/HA composite conversion coating on the extruded Mg-2Zn-1Mn-0.5Ca alloy for bone implant application, Surf. Coat. Technol. 325 (2017) 127–135.

[53] X. Zhan, W. Shang, Y. Wen, Y. Li, M. Ma, Preparation and corrosion resistance of a three-layer composite coatings on the Mg alloy, J. Alloys Compd. 774 (2019) 522–531.

[54] L.-Y. Cui, G.-B. Wei, Z.-Z. Han, R.-C. Zeng, L. Wang, Y.-H. Zou, S.-Q. Li, D.-K. Xu, S.-K. Guan, In vitro corrosion resistance and antibacterial performance of novel tin dioxide-doped calcium phosphate coating on degradable Mg-1Li-1Ca alloy, Journal of Materials Science & Technology 35 (2019) 254–265.

[55] V. Kavimani, K.S. Prakash, R. Gunashri, P. Sathish, Corrosion protection behaviour of r-GO/TiO_2 hybrid composite coating on magnesium substrate in 3.5 wt.% NaCl, Progress in Organic Coatings 125 (2018) 358–364.

[56] J. Chen, W. Lin, S. Liang, L. Zou, C. Wang, B. Wang, M. Yan, X. Cui, Effect of alloy cations on corrosion resistance of LDH/MAO coating on magnesium alloy, Appl. Surf. Sci. 463 (2019) 535–544.

[57] L.-Y. Cui, S.-D. Gao, P.-P. Li, R.-C. Zeng, F. Zhang, S.-Q. Li, E.-H. Han, Corrosion resistance of a self-healing micro-arc oxidation/polymethyltrimethoxysilane composite coating on magnesium alloy AZ31, Corros. Sci. 118 (2017) 84–95.

[58] S. Wang, H. Peng, Z. Shao, Q. Zhao, N. Du, Sealing of anodized aluminum with phytic acid solution, Surf. Coat. Technol. 286 (2016) 155–164.

[59] A.D. King, N. Birbilis, J.R. Scully, Accurate electrochemical measurement of magnesium corrosion rates; a combined impedance, mass-loss and hydrogen collection study, Electrochim. Acta 121 (2014) 394–406.

[60] R. Babilas, A. Bajorek, W. Simka, D. Babilas, Study on corrosion behavior of Mg-based bulk metallic glasses in NaCl solution, Electrochim. Acta 209 (2016) 632–642.

[61] L.-X. Li, Z.-H. Xie, C. Fernandez, L. Wu, D. Cheng, X.-H. Jiang, C.-J. Zhong, Development of a thiophene derivative modified LDH coating for Mg alloy corrosion protection, Electrochim. Acta 330 (2019) 135186.

[62] M.P. Gomes, I. Costa, N. Pébère, J.L. Rossi, B. Tribollet, V. Vivier, On the corrosion mechanism of Mg investigated by electrochemical impedance spectroscopy, Electrochim. Acta 306 (2019) 61–70.

[63] M.C. Delgado, F.R. García-Galvan, I. Llorente, P. Pérez, P. Adeva, S. Feliu, Influence of aluminium enrichment in the near-surface region of commercial twin-roll cast AZ31 alloys on their corrosion behaviour, Corros. Sci. 123 (2017) 182–196.

[64] J. Chen, J. Wang, E. Han, J. Dong, W. Ke, AC impedance spectroscopy study of the corrosion behavior of an AZ91 magnesium alloy in 0.1M sodium sulfate solution, Electrochim. Acta 52 (2007) 3299–3309.

[65] R. Yan, T. Liang, H.C. Ren, J. Gu, Z.Z. Ji, Study on corrosion behaviors of epoxy aluminum coating immersed in 3.5% NaCl solution, Adv. Mater. Res. 912–914 (2014) 338–341.

[66] J. Li, B. Zhang, Q. Wei, N. Wang, B. Hou, Electrochemical behavior of Mg-Al-Zn-In alloy as anode materials in 3.5 wt.% NaCl solution, Electrochim. Acta 238 (2017) 156–167.

[67] L. Ganborena, J.M. Vega, B. Özkaya, H.-J. Grande, E. García-Lecina, AN SKP and EIS study of microporous nickel-chromium coatings in copper containing electrolytes, Electrochim. Acta 318 (2019) 683–694.

[68] X. Wang, L. Li, Z.-H. Xie, G. Yu, Duplex coating combining layered double hydroxide and 8-quinolinol layers on Mg alloy for corrosion protection, Electrochim. Acta 283 (2018) 1845–1857.

[69] F.S.d. Silva, J. Bedoya, S. Dosta, N. Cinca, I.G. Cano, J.M. Guilemany, A.V. Benedetti, Corrosion characteristics of cold gas spray coatings of reinforced aluminum deposited onto carbon steel, Corros. Sci. 114 (2017) 57–71.

[70] C. Ma, X. Liu, C. Zhou, Cold-sprayed Al coating for corrosion protection of sintered NdFeB, J. Therm. Spray Technol. 23 (2013) 456–462.

[71] A. Farooq, M. Hamza, Q. Ahmed, K.M. Deen, Evaluating the performance of zinc and aluminum sacrificial anodes in artificial seawater, Electrochim. Acta 314 (2019) 135–141.

[72] Y.-K. Wei, X.-T. Luo, Y. Ge, X. Chu, G.-S. Huang, C.-J. Li, Deposition of fully dense Al-based coatings via in-situ micro-forging assisted cold spray for excellent corrosion protection of AZ31B magnesium alloy, J. Alloys Compd. 806 (2019) 1116–1126.

[73] M. Santamaria, F. Di Quarto, S. Zanna, P. Marcus, Initial surface film on magnesium metal: a characterization by X-ray photoelectron spectroscopy (XPS) and photocurrent spectroscopy (PCS), Electrochim. Acta 53 (2007) 1314–1324.

[74] M.A. Amin, S.S. Abd El Rehim, S.O. Moussa, A.S. Ellithy, Pitting corrosion of Al and Al-Cu alloys by $ClO4^-$ ions in neutral sulphate solutions, Electrochim. Acta 53 (2008) 5644–5652.